

---

# Shadow detection and correction using a combined 3D GIS and image processing approach

Safa Ridene<sup>1</sup>, Reda Yaagoubi<sup>1</sup>, Imane Sebari<sup>1</sup>,  
Audrey Alajouanine<sup>2</sup>

1. College of Geomatics and Surveying Engineering, Institut Agronomique et Vétérinaire Hassan II, Rabat, Morocco

2. GE-INFRA, Géomètre Expert, Toulouse  
[Reda.yaagoubi@iav.ac.ma](mailto:Reda.yaagoubi@iav.ac.ma); [i.sebari@iav.ac.ma](mailto:i.sebari@iav.ac.ma)

---

**ABSTRACT.** While shadow can give useful information about size and shape of objects, it can pose problems in feature detection and object detection, thereby, it represents one of the major perturbator phenomena frequently occurring on images and unfortunately, it is inevitable. “Shadows may lead to the failure of image analysis processes and also cause a poor quality of information which in turn leads to problems in implementation of algorithms.” (Mahajan and Bajpayee, 2015). It also affects multiple image analysis applications, whereby shadow cast by buildings deteriorate the spectral values of the surfaces. Therefore, its presence causes a deterioration in the visual image’s quality and limits the information that the former could give. Ignoring the existence of shadows in images may cause serious problems in various visual processing applications such as false objects detection. In this context, many researches have been conducted through years. However, it is still a challenge for analysts all over the world to find a fully automated and efficient method for shadow removal from images.

**RÉSUMÉ.** Alors que l’ombre peut donner des informations utiles sur la taille et la forme des objets, elle peut poser des problèmes dans la détection de caractéristiques et d’objets, elle représente donc l’un des principaux phénomènes perturbateurs se produisant fréquemment sur les images mais elle est inévitable. « Les ombres peuvent conduire à l’échec des processus d’analyse d’image et aussi causer une mauvaise qualité de l’information qui à son tour conduit à des problèmes dans la mise en œuvre des algorithmes. » (Mahajan et Bajpayee, 2015). Elle affecte également de multiples applications d’analyse d’images, où l’ombre projetée par les bâtiments détériore les valeurs spectrales des surfaces. Sa présence entraîne donc une détérioration de la qualité de l’image visuelle et limite l’information que celle-ci peut fournir. Ignorer l’existence d’ombres dans les images peut causer de sérieux problèmes dans diverses applications de traitement visuel telles que la détection de faux objets. Dans ce contexte, de nombreuses recherches ont été menées au fil des ans. Cependant, les analystes du monde entier ont encore du mal à trouver une méthode entièrement automatisée et efficace pour l’élimination des ombres sur les images.

**KEYWORDS:** 3D GIS, image processing, modelbuilder, multipatch, orthophoto, shadow.

**MOTS-CLÉS :** SIG 3D, traitement d’images, modelbuilder, multipatch, orthophoto, ombre.

---

DOI: [10.3166/ig.2019.00091](https://doi.org/10.3166/ig.2019.00091) © 2019 Lavoisier

## 1. Extended abstract

Shadow has always been an issue for a plethora of image processing applications. Since, its presence deteriorates the visual quality of the image, which results in a loss in information that can be drawn from it.

Thus, this work presents an effort to contribute a new solution for an old challenge, an automatic method for cast shadow detection and compensation from orthophotos using a conjunction between 3D GIS and image processing. In a first phase, the outline of the developed process involves a new workflow that aims to use 3D GIS technology to detect cast shadow appearing on orthophotos. This new workflow was divided into four sub-steps. First, we needed to extract building footprints from LIDAR data. Then, we used 3D GIS technology to generate building multipatch and to calculate the shadow volumes that we used afterwards to create a shadow mask that points out the shadow regions existing on the orthophoto. In a second phase, we used an image-processing algorithm that aims to compensate the shadowed regions. We applied it on the whole image including its already non-shadowed regions. Then, we integrated the already determined shadow mask to replace the shadowed regions with their equivalent after compensation, to obtain at last, the desired outcome which is a de-shadowed orthophoto.

To evaluate the performance of the proposed methodology, evaluation metrics involved in shadow detection and compensation techniques were calculated. We obtained an F-score of 97% considering that our proposed methodology was basically designed for shadow cast by buildings. In short, in this project, we focused on delivering a new approach that combines 3D GIS for the cast shadow detection and image processing algorithms for shadow compensation.

## 2. Introduction

Over the years, orthophotos have become one of the most used resources to satisfy a huge number of needs namely basic and thematic cartography. Hence, this report will investigate the complementarity between geographic information systems and the image processing techniques to figure out a new solution for an old, persistent problem which is the existence of shadow. “Shadow represents an important problem for both, users and sellers of remote sensing images.” (Massalabi *et al.*, 2004). It directly effects the scene’s illumination, thereby, it represents one of the major factors affecting the performance of multiple computer vision applications, namely: Image matching, image segmentation (Vazquez, 2008), change detection, object detection and tracking, traffic monitoring and surveillance.

## 3. Methodology

### 3.1. Study area and dataset

Since the workflow is basically designed for building’s shadow, an urban area was chosen as a study area. This area encompasses the majority of high buildings and present important cast shadows (Figure 1).

3.1.1. LAS data



Figure 1. Study Area

LiDAR data of the city of Toulouse (France) was stored using the LAS format. The LAS file is intended to contain LIDAR point cloud data records. It was initially collected in 2017 using the RGF1993 coordinate system, based on a Lambert Conformal Conic Projection (Figures 2 and 3).



Figure 2. LAS dataset extent of the study area



Figure 3. Part of a LAS tile within the study area

### 3.1.2. Shapefile limits

Another test data that we used during this workflow was the shapefile limits of images. They were represented by polygons that describe the limits of each image. They were used to make it possible to assign to each shapefile limit its corresponding date and time of acquisition.

### 3.1.3. Time Stamps

Calculating shadow features was based on the solar data, more particularly, the date and time of acquisition. The date and time information were issued from the flight report provided by the host company.

The flight report gives date and time for each flight line. Therefore, it was necessary to format date time information into a standard date-time format (such as MM/DD/YYYY HH:MM:SS AM) (Figure 4).

Line,	Start time	End time
1,	12/08/2017 07:48 AM,	12/08/2017 07:55 AM
2,	12/08/2017 08:07 AM,	12/08/2017 08:12 AM
3,	12/08/2017 07:51 AM,	12/08/2017 07:57 AM

Figure 4. Time stamp text file sample

### 3.1.4. Orthophoto

Another used data is an orthophoto in the region of Toulouse (France). It has as a resolution of 5 cm. It was taken in August 2017 using the RGF93 coordinate system, based on a Lambert Conformal Conic Projection (Figure 5).



Figure 5. Orthophoto

3.2. Shadow determination workflow

In order to implement our 3D GIS solution, we will adopt the proposed methodology presented in Figure 6.

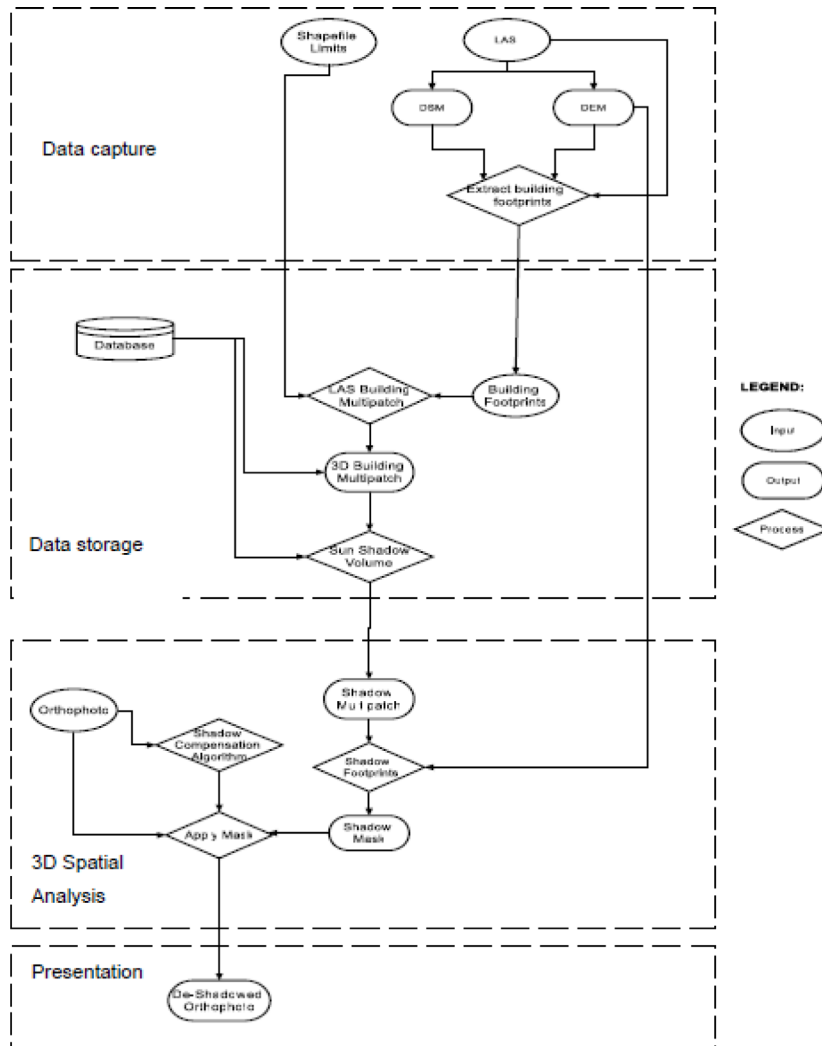


Figure 6. Flowchart of the proposed methodology

Building footprints information is crucial for our shadow determination workflow (Figure 7). They are a representation of the area of ground covered when viewed from directly above (Crowley, 2011).

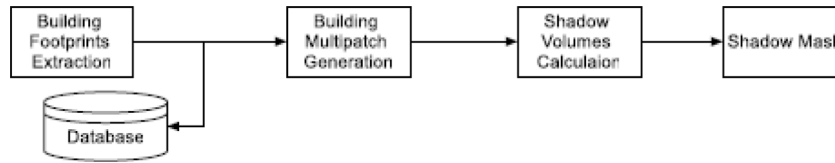


Figure 7. Shadow determination flowchart

Then, we focused on the 3D reconstruction of building models from LIDAR data and 2D building footprints. Which means, we considered a data-structure based approach for building modeling. Also called data-driven or bottom-up, this approach does not use any predetermined building model but tries to find planes in the LIDAR point clouds and group them into buildings (Schwalbe, 2005).

Data model and data structure are the basic contents for spatial data organization, and they are the keys for GIS software development. Conceptual model is a core of spatial data model design, which is used to define some rules for representing attributes of spatial model (Yanbing, 2007).

In order to implement our 3D GIS solution, the proposed conceptual data model contained the following classes, which are.

- Frames: each frame correspond to a specific start/end time of acquisition, azimuth and latitude.
- Footprints: each footprint correspond to a building. They are in 2D geometry.
- Buildings: each building correspond to only one footprint. They are in 3D geometry.
- Shadow volumes: each building can produce 0 or many shadow volumes. They are in 3D geometry.

The equivalent figure shows the considered conceptual model (Figure 8):

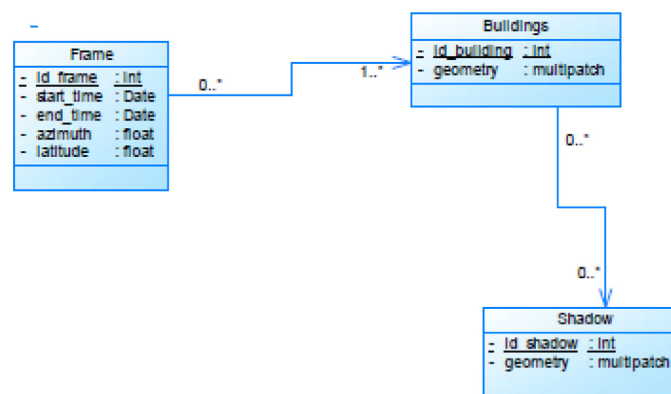


Figure 8. Conceptual Data Model

### 3.3. Shadow compensation

Once the location of shadows is given, figuring out a method to compensate it would be an easy task. (Finlayson *et al.*, 2009) pointed to the fact that the shadow and non-shadow regions differ by a single constant, which can be calculated for R, G and B channels separately. The constant, once added to the shadow region, will reduce the difference between the shadow region and the background.

We started by determining the averages of each channel in both shadow and non-shadow regions. Then, we calculated the following ratios for each channel.

$$C_r = S_r/nS_r \quad (1)$$

$$C_g = S_g/nS_g \quad (2)$$

$$C_b = S_b/nS_b \quad (3)$$

Where:  $C_r, C_g, C_b$ : Constants for each channel ;

$S_g, S_b$ : average of each channel in shadow regions;

$nS_r, nS_g, nS_b$ : average of each channel in non-shadow regions

After that, we proceeded with multiplying each channel by its corresponding constant.

$$c_1 = r * C_r \quad (4)$$

$$c_2 = g * C_g \quad (5)$$

$$c_3 = b * C_b \quad (6)$$

At this level, we applied the compensation algorithm on the whole image. Afterwards, we used another algorithm to replace the shadowed regions on the original orthophoto by their equivalent compensated regions (Figure 9).

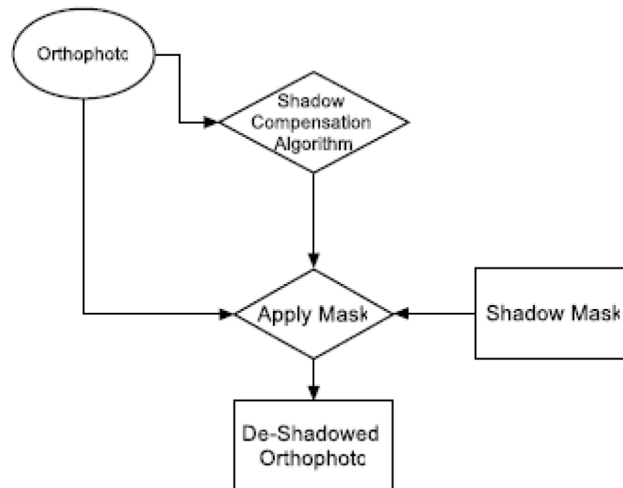


Figure 9. Shadow Compensation Steps

As shown in the following figure, we started by performing the correction algorithm on the whole image. Then, we replaced the shadowed regions by their equivalent enhanced ones based on our shadow mask.

This method was implemented within MATLAB, to obtain, at least, the desired shadow-free orthophoto.

#### 4. Results and Analysis

At a first time, we will present the results. Afterwards, we will go further into details by evaluating the proposed method and explaining the problems that appeared while doing this work. Finally, we will enclose this chapter by mentioning its drawn conclusions as well as some recommendations for a better use of the proposed method.

##### 4.1. Results

The following figure shows the final result of the shadow determination workflow. We obtained a binary shadow mask where each pixel is assigned a value of either 1 (shadow) or 0 (non-shadow) (Figure 10).



*Figure 10. Results of the shadow detection. Original image (left)  
Shadow mask (right)*

The next figure shows the result of the shadow compensation process. Based on the determined shadow mask, we applied a compensation algorithm to relight each pixel. To obtain at last, a shadow-free orthophoto ([Figure 11](#)).



*Figure 11. Results of the shadow compensation. Original image (left).  
Result of our proposed method (right)*

## **4.2. Performance evaluation**

### **4.2.1. Shadow detection evaluation**

For the shadow detection evaluation, we used the same metrics and accuracy table from ([Tsai, 2006](#)). Which are the four well-known metrics: Producer's accuracy, user's accuracy, overall accuracy and F-score to evaluate the shadow detection results.

The producer's accuracy – also known as recall – measures how well the method detects the true shadowed from the non-shadowed pixels.

$$\tau_s = \frac{TP}{TP + FN} \quad (7)$$

$$\tau_n = \frac{TN}{TN + FP} \quad (8)$$

Where:

- $\tau_s$  = The producer's accuracy of the shadowed pixels.
- $\tau_n$  = The producer's accuracy of the non-shadowed pixels.
- The true positive (TP) = Number of shadowed pixels correctly classified as shadow.
- True negative (TN) = Number of non-shadowed pixels correctly detected and identified as non-shadow.
- False negative (FN) = Number of shadow pixels judged as non-shadow.
- False positive (FP) = Number of non-shadow pixels falsely detected as shadow.
- The user's accuracy – also known as precision – is used to measure the precision of the algorithm and indicate the probabilities of correctly detected shadowed and non-shadowed pixels.

$$\sigma_s = \frac{TP}{TP + FN} \quad (9)$$

$$\sigma_n = \frac{TN}{TN + FP} \quad (10)$$

Where  $\sigma_s$  represents the user's accuracy of the shadowed pixels and  $\sigma_n$  represents the user's accuracy of the non-shadowed pixels.

The proposed methodology for shadow detection is basically designed for shadow cast by buildings. However, in the shadow mask determination process, we could not prevent some trees' shadow from coming in.

In order to point out our proposed methodology's efficiency, we applied the accuracy test in two cases. Case 1 in which we involved the trees and case 2 in which we set the trees to nodata (Tables 1 and 2).

Table 1. Shadow detection accuracy measurements of our proposed method (case 1)

Producer's Accuracy (%)		User's Accuracy (%)		Overall Accuracy (%)	F-Score (%)
$\tau_s$	$\tau_n$	$\sigma_s$	$\sigma_n$	$\rho$	F
86	93	58	98	93	69

Table 2. Shadow detection accuracy measurements of our proposed method (case 2)

Producer's Accuracy (%)		User's Accuracy (%)		Overall Accuracy (%)	F-Score (%)
$\tau_s$	$\tau_n$	$\sigma_s$	$\sigma_n$	$\rho$	F
95	90	99	61	95	97

#### 4.2.2. Shadow compensation evaluation

To evaluate the quality of the used shadow enhancement algorithm, we used three-color histograms for R, G and B, in a lit region of the road, at a first time, to better understand the distribution of the three channels that we are expecting from our shadow enhancement algorithm. So, basically, the first histogram was used as a reference. Then, we used the histograms of a road region before and after enhancement, to get to see the difference in the distribution of the three channels (Figure 12).

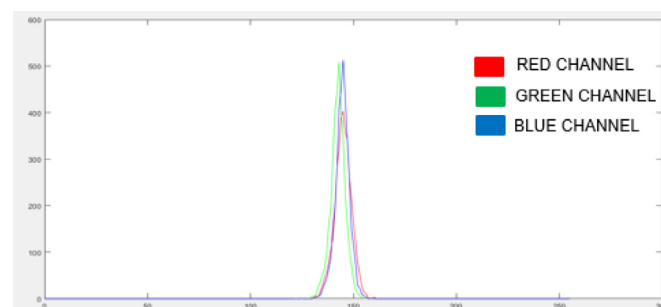


Figure 12. Histogram of lit region of the road

A three-color histogram shows the brightness distribution for each color individually. It is considered the best tool to understand the distribution of an image intensities. In Figure 13, we can see that the three channels have a spike on the left hand side of the histogram, which can be explained by the presence of shadow and that the concerned region is under exposed. However, in Figure 14, all of the three channels are right in the middle of the histogram, which means that the concerned region is correctly exposed.

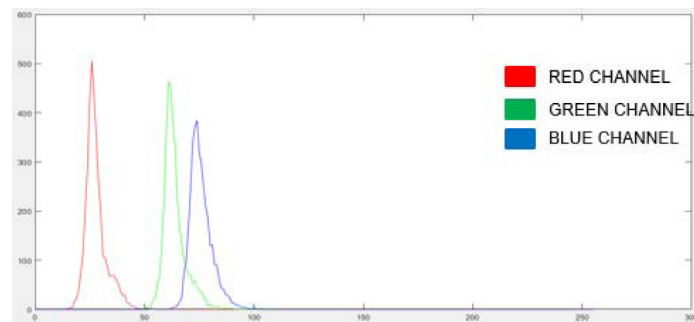


Figure 13. Histogram of shadowed region of the road before compensation

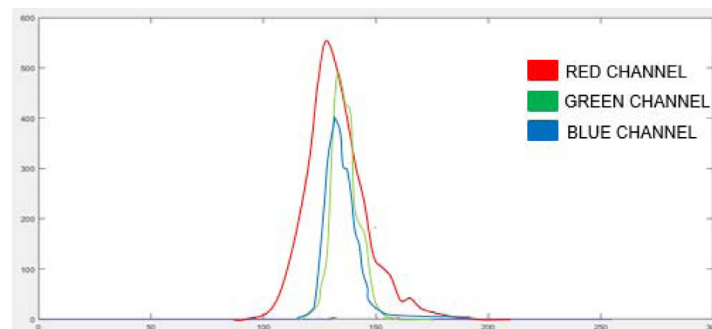


Figure 14. Histogram of shadowed region of the road after compensation

## 5. Conclusion

Though our proposed method outperform so many methods in the literature overview, it still has several limitations. It mainly works well in urban areas. And it may not be up to expectations in some conditions for example, when it comes to trees. Since it is designed for removing shadow cast by buildings, it is not capable of giving a correct and exact shadow tree removal. Which is why there were some visually noticeable

artifacts in the final result. Hence, it can be anticipated that future work will be done to enhance 3D tree reconstruction. Another modification that is highly recommended is to consider using an algorithm for shadow boundaries smoothing to reduce the over-illumination that may occur towards the edges of shadow. We also recommend focusing on modeling shadow cast by trees and why not self-shadow.

### **Bibliographie**

- Crowley J. (2011). *City of Redlands Safe Routes to Schools Shadow Mapping*.
- Finlayson G., Drew M., Lu C. (2009). Entropy Minimization for Shadow Removal. *Int. J. Comput. Vision*, vol. 85, n° 1, p. 35-57.
- Mahajan R., Bajpayee A. (2015). A survey on shadow detection and removal based on single light source. *IEEE Sponsored 9th International Conference on Intelligent Systems and Control (ISCO)*.
- Massalabi A., Dong-Chen H., Benie G., Beaudry E. (2004). Detecting information under and from shadow in panchromatic IKONOS images of the city of Sherbrooke. *In Proc. IGARSS, Anchorage, AK, USA*, vol. 3, p. 2000-2004.
- Schwalbe E.M.-G. (2005). 3D building generation from airborne laser scanner data using 2D GIS data and orthogonal point cloud projections. *Workshop ISPRS laser scanning, Enschede, the Netherlands*.
- Tsai V.J. (2006). A comparative study on shadow compensation of color aerial images in invariant color models. *IEEE transactions on geoscience and remote sensing*, 44, n° 6, p. 1661-1671.
- Vazquez E. (2008). Colour image segmentation in presence of shadow. *In Conference on Colour in Graphics, Imaging, and Vision*, n° 1, p. 383-387.
- Yanbing W.L. (2007). On 3D GIS spatial modeling. In ISPRS Workshop on Updating Geo-spatial Databases with Imagery & The 5th ISPRS Workshop on DMGISs. ISPRS.